JOURNAL OF CLIMATE

Dynamic and energetic constraints on the modality and position of the intertropical convergence zone in an aquaplanet

ORI ADAM*

The Fredy and Nadine Herrmann Institute of Earth Sciences, The Hebrew University, Jerusalem, Israel

ABSTRACT

The tropical zonal-mean precipitation distribution varies between having single or double peaks, which are associated with intertropical convergence zones (ITCZs). Here, the effect of this meridional modality on the sensitivity of the ITCZ to hemispherically-asymmetric heating is studied using an idealized GCM with parameterized Ekman ocean energy transport (OET). In the idealized GCM, transitions from unimodal to bimodal distributions are driven by equatorial ocean upwelling and cooling, which inhibits equatorial precipitation. For sufficiently strong equatorial cooling, the tropical circulation bifurcates to anti-Hadley circulation in the deep tropics, with a descending branch near the equator and off-equatorial double ITCZs. The intensity and extent of the anti-Hadley circulation is limited by a negative feedback: westerly geostrophic surface wind tendency in its poleward lower branches balances the easterly stress (and hence equatorial upwelling) required for its maintenance. For weak ocean stratification, which goes along with unimodal or weak bimodal tropical precipitation distribution, OET damps shifts of the tropical precipitation centroid but amplifies shifts of precipitation peaks. For strong ocean stratification, which goes along with pronounced double ITCZs, asymmetric heating leads to relative intensification of the precipitation peak in the warming hemisphere, but negligible meridional shifts. The dynamic feedbacks of the coupled system weaken the gradient of the atmospheric energy transport (AET) near the equator. This suggests that over a wide range of climates, the ITCZ position is proportional to the cubic root of the cross-equatorial AET, as opposed to the commonly-used linear relation.

1. Introduction

The atmospheric Hadley circulation, characterized by ascent in the deep tropics and descent in the subtropics, is complemented by the zonal-mean wind-driven shallow oceanic subtropical cells (STCs), with upwelling near the equator and downwelling at higher latitudes (McCreary and Lu 1994; Held 2001; Czaja and Marshall 2006; Schneider et al. 2014; Green and Marshall 2017). The coupled momentum and energy budgets of the oceanic and atmospheric tropical overturning circulations determine the emergent properties of these circulations, such as the tropical rain belt (Schneider et al. 2014; Byrne et al. 2018; Kang 2020). Here, the relation of the coupled tropical overturning circulation to the zonal-mean tropical precipitation distribution is studied using an idealized GCM that allows isolating aspects of the dynamic coupling between the atmosphere and ocean.

The intertropical convergence zone (ITCZ), where the surface branches of the northern and southern Hadley cells converge, is generally identified as the latitude of maximal tropical precipitation. However, in both observations and simulations, the zonal-mean tropical precipitation distribution is often doubly peaked (Zhang 2001). In observations, the doubly-peaked precipitation distribution is primarily due to pronounced rain bands in the Pacific both north and south of the equator[1] (Schneider et al. 2014). Doubly-peaked tropical precipitation also appear in simulations with idealized boundary conditions such as aquaplanet simulations (e.g., Sumi 1992; Voigt et al. 2014b; Popp and Silvers 2017), and are often excessively represented in modern climate models[2] (Mechoso et al. 1995; Lin 2007; Adam et al. 2016c). The doubly-peaked precipitation distribution, albeit inconsistent with the expectation of a single ITCZ in the Hadley circulation, is commonly referred to as a 'double ITCZ'. This terminology is maintained here in describing the zonal-mean precipitation, referring to single peaks as ITCZs, pairs of peaks as double ITCZs (IITCZs for short), and the rising branch of the Hadley circulation as 'the ITCZ'.

What determines the modality of the zonal-mean tropical precipitation distribution? Tropical precipitation

*Corresponding author address: Ori Adam, The Hebrew University, Jerusalem, Israel.
E-mail: ori.adam@mail.huji.ac.il

[1]The rain band north of the equator is commonly referred to as the Pacific ITCZ whereas the southern rain band, mostly confined to the western Pacific, is referred to as the south Pacific convergence zone (SPCZ).

[2]A tendency commonly known as the 'double ITCZ bias'.

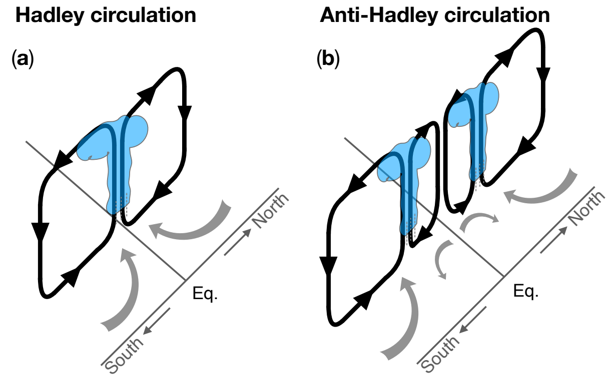

FIG. 1. A depiction of the atmospheric meridional overturning circulation, the geostrophic component of the surface winds and the ITCZ positions for (**a**) Hadley circulation (single ITCZ), and (**b**) anti-Hadley circulation (double ITCZs).

generally peaks near maximal sea surface temperatures (SSTs)[3], which drive surface convergence (Lindzen and Nigam 1987; Back and Bretherton 2009). Philander et al. (1996) pointed to the dynamic coupling between the surface winds associated with the ITCZ and the wind-driven ocean circulation. The wind-driven equatorial ocean upwelling leads to an equatorial cold tongue; the cold tongue, in turn, inhibits precipitation near the equator, forcing the precipitation distribution to either be doubly peaked about the equator, or be single-peaked in the hemisphere with warmer tropical waters. Thus, the emergence of IITCZs and the positions of ITCZs are inextricably linked to the dynamic coupling between the tropical atmospheric and oceanic overturning circulations.

Bischoff and Schneider (2016) provided energetic constraints on the modality of the zonal mean precipitation distribution. They showed that IITCZs can emerge when a deficit exists in the equatorial atmospheric energy budget, requiring convergence of energy into the equatorial latitudes. Since atmospheric energy transport (AET) in the tropics follows the upper branch of the circulation, the net convergence of energy at the equator by the mean circulation drives an equatorial descending branch, and two rising branches on either side of the equator where the IITCZs reside – effectively forming an 'anti-Hadley' circulation in the deep tropics (Fig. 1). Consistent with these equatorial energetic constraints, the observed transition to IITCZ states in the eastern Pacific during boreal spring is found to occur during an equatorial energetic deficit in the eastern Pacific sector (Adam et al. 2016b). In aquaplanet simulations, IITCZ states have been shown to emerge when an equatorial energetic deficit is forced by, for example, increased equatorial ocean heat uptake (Bischoff and Schneider 2016) or by cloud radiative effects (Voigt et al. 2014a; Talib et al. 2018). Transitions between ITCZ and IITCZ states are also known to be sensitive to convective parameterization, generally favoring IITCZ states with weakened convective mixing (e.g., Möbis and Stevens 2012; Talib et al. 2018). Under zonally asymmetric conditions, regional IITCZs can emerge adjacent to the descending branches of tropical zonal overturning circulations if mechanical damping is sufficiently strong (Adam 2018; Popp and Bony 2019).

Common to the mechanisms described above is the key role of the coupled equatorial energy and momentum budgets in setting the modality of the zonal mean precipitation distribution. Similarly, the coupled equatorial energy and momentum budgets have a critical role in setting the position of the ITCZ, which tends to lie in the warmer hemisphere. Meridional migrations of the ITCZ, driven by hemispherically asymmetric heating, are modulated by the atmospheric net energy input (NEI) at the equator (Bischoff and Schneider 2014; Schneider et al. 2014; Adam et al. 2016a), which affects both the sensitivity of the ITCZ to hemispherically asymmetric heating and the distribution of tropical SSTs. Since shifts of the ITCZ lead to changes in the tropical zonal-mean wind stress, which drives the oceanic STCs and their associated ocean energy transport (OET) and heat uptake, the coupled equatorial energy and momentum budgets are linked to both the modality and position of the ITCZ in a complex manner. This complex interaction is the focus of the present analysis.

Figure 2a shows the observed zonal-mean atmospheric NEI (solid black), given by the sum of the net radiative input at the top of the atmosphere, and the net surface energy flux into the atmosphere – the latter generally dominated by ocean heat uptake in the tropics (Schneider et al. 2014). A striking feature of the atmospheric NEI is its equatorial minimum, caused by the increased ocean heat uptake at the equatorial cold tongues of the Pacific and Atlantic (leading also to an equatorial SST minimum, as shown in Fig. 2b), which is reinforced by cloud radiative feedbacks (e.g., Hartmann 1994; Philander et al. 1996; Voigt et al. 2014a). While the observed cold tongues of the Pacific and Atlantic are strongly related to the zonal overturning circulations in these basins (i.e., the Bjerknes feedback; Bjerknes 1969), ocean Ekman upwelling can lead to similar zonally-uniform equatorial cooling in aquaplanets (Fig. 2a; Medeiros et al. 2015), associated with the zonal-mean STCs. The minimum in the equatorial zonal-mean NEI and SST disappears when the wind-driven equatorial upwelling is suppressed, as is the case in static slab ocean models (Fig. 2, magenta line; Smith et al. 2006; Codron 2012), and is significantly diminished in coupled models with a sufficiently deep thermocline[4] (e.g., Philander

[3]More generally, convective quasi equilibrium predicts maximal deep convection above maximal values of the moist entropy of the subcloud layer (Emanuel 2005; Privé and Plumb 2007), which approximately follows SSTs.

[4]This is evident by the change in the sea surface temperature, which closely follows NEI in the deep tropics (Adam et al. 2018a).

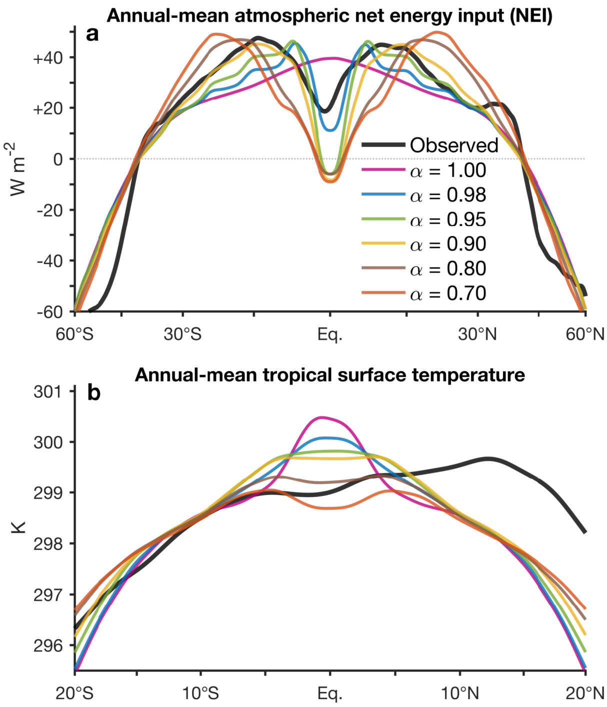

FIG. 2. The annual-mean zonally averaged (**a**) atmospheric net energy input (NEI) and (**b**) tropical surface temperature in the observed climate (thick black), and in the idealized GCM (colors) for varying ocean stratification values (α). The α=1 line (magenta) corresponds to a static slab ocean (i.e., without wind-driven ocean energy transport). Observed values are taken from the European Center for Medium-Range Weather Forecasts (ECMWF) Interim Reanalysis (Dee et al. 2011) for the years 1979–2014. GCM surface temperatures are reduced by 7K to match mean tropical observed values.

and Fedorov 2003; Zheng et al. 2012); it can also exist to some degree purely due to convective dynamics (Möbis and Stevens 2012; Blackburn et al. 2013; Medeiros et al. 2015). Thus, while the exact equatorial energy balance is determined by a slew of mechanisms associated with radiative and dynamic feedbacks, the existence of the equatorial minimum in the observed atmospheric NEI is primarily due to the equatorial cooling by wind-driven ocean upwelling. This study therefore focuses on the role of the wind-driven ocean circulation in setting the tropical energy and momentum balances, and its effect on the tropical zonal-mean precipitation distribution. Cloud radiative effects, zonal asymmetries and ocean eddy momentum and heat fluxes, which have important roles in the tropical energy and momentum budgets (e.g., Bjerknes 1969; Philander et al. 1996; Swenson and Hansen 1999; Philander and Fedorov 2003; Dima et al. 2005; Trenberth and Fasullo 2012), are neglected in the present analysis.

The application of both dynamic and energetic constraints has been shown to provide valuable insights on ITCZ dynamics. Schneider et al. (2014) argued that the wind-driven STCs, which transport energy in the same direction as the Hadley circulation (Held 2001), reduce the burden on atmospheric energy transport (AET) and therefore damp ITCZ shifts in response to hemispherically asymmetric heating. Subsequent works, which isolated the role of wind-driven OET, supported the assumption of damped ITCZ shifts due to the partitioning of energy transport between the atmosphere and oceans (Green and Marshall 2017; Schneider 2017; Kang et al. 2018b,a; Green et al. 2019; Lutsko et al. 2019; Gerstman and Adam 2020). Specifically, Kang et al. (2018a) found that Ekman transport only partly accounts for the damping found in fully coupled models, suggesting processes associated with deep ocean circulation, the subtropical gyres and ocean heat uptake are important. Indeed, Yu and Pritchard (2019) found that the Atlantic meridional overturning circulation (AMOC) has a critical role in the coupled response (for an extended discussion of how these circulations are linked, see Barreiro et al. 2008). Gerstman and Adam (2020) found a nonlinear dependence of ITCZ shifts on ocean stratification and asymmetric heating, that allowed a parameter range where damping comparable to that seen in fully coupled models can be achieved solely by Ekman energy transport. Moreover, they found that for relatively weak asymmetric heating, non-monotonic response of atmospheric transient eddies can lead to amplified ITCZ shifts.

The present analysis aims to extend our understanding of how wind-driven OET affects the modality of the zonal-mean tropical precipitation distribution, and of how variations in the precipitation modality affect ITCZ shifts. To isolate the role of the zonal-mean wind-driven ocean circulation, an idealized atmospheric GCM is used, coupled to a slab ocean model with parameterized Ekman energy transport. The idealized coupled model is similar to those employed by Kang et al. (2018a,b), Lutsko et al. (2019) and Gerstman and Adam (2020), who successfully isolated the effects of the wind-driven Ekman energy transport on shifts of the ITCZ. As in these studies, the sensitivity of the zonal-mean tropical precipitation distribution to prescribed hemispherically asymmetric heating and ocean stratification is examined. This provides valuable insight into the zonal-mean tropical precipitation response to hemispherically asymmetric forcing caused by, for example, volcanic eruptions (Colose et al. 2016; PAGES Hydro2k Consortium 2017) and the slowdown of AMOC in response to freshening of the northern Atlantic (Barreiro et al. 2008); it also provides insight on the sensitivity to variations in tropical ocean stratification, such as, for example, the shoaling of the tropical thermocline during the Quaternary (Philander and Fedorov 2003) and thermocline depth biases in modern climate models (Zheng et al. 2012). While limited in its scope (see review by Kang 2020), the idealised model is found to capture essential elements of the coupled dynamics, which can be used to interpret observations and inform more complex models.

The model and methods are described in Section 2. In Sections 3 and 4, dynamic and energetic constraints on the modality and position of the ITCZ are presented, followed by a Discussion and summary in section 5.

2. Model and methods

The numerical model and simulation setup used here are similar to those used in Gerstman and Adam (2020), differing only in the values of a few key parameters, as described below. See Gerstman and Adam (2020) for a derivation of the Ekman mass transport, and Codron (2012) for more details on the Ekman energy transport scheme.

a. Model description

The idealized GCM is based on the spectral dynamical core of the Geophysical Fluid Dynamics Laboratory (GFDL) flexible modeling system. The radiative and convective schemes used in the model are described in Frierson et al. (2006) and in O'Gorman and Schneider (2008). The model code is publicly available at *https://github.com/tapios/fms-idealized*.

The idealized GCM is run with a T42 horizontal resolution, 18 unevenly spaced σ levels and an ocean mixed-layer depth of 50 m. A two-stream gray radiation scheme is used, with prescribed meridional profiles of longwave absorption (longwave absorption parameters of 1.8 and 7.2 at the poles and at the equator, respectively; cf. O'Gorman and Schneider 2008). Moist processes are represented by relaxation of the temperature profile to a convective radiative-equilibrium state (Schneider 2004), and relaxation of the relative humidity to a reference state of 70% using a simplified Betts-Miller Scheme. The results show time averages of 1000 days, following spin ups of 5000 days.

b. Ekman energy transport

The wind-driven ocean energy transport (OET) is based on the two-layer model described in Codron (2012), where the net transport is given by the difference between the surface and deep layers. The wind-driven ocean heat uptake is given by

$$\nabla \cdot F^{Ek} = -\frac{C}{a\,\cos(\phi)}\frac{\partial}{\partial\phi}\left(M_y(T_s - T_d)\cos(\phi)\right) \tag{1}$$

where F^{Ek} is the ocean Ekman energy transport, a is Earth's radius, C=3989.2 J kg^{-1} K^{-1} is the specific heat capacity of the ocean and ϕ denotes latitude. The difference between the surface and deep ocean layer temperatures, $T_s - T_d$, is given by

$$T_s - T_d = (T_s - T_o)(1-\alpha) \tag{2}$$

where T_o=271.3K is the freezing temperature of seawater and the parameter α controls the thermal stratification of the wind-driven circulation, with zero OET and ocean heat uptake for $\alpha = 1$. In this model, $T_s - T_d$ in the tropics (20°S–20°N) varies linearly with α, and is well approximated by $T_s - T_d = 33.6(1-\alpha)$K with negligible dependence on hemispherically asymmetric heating. The Ekman mass transport M_y is given by (Gerstman and Adam 2020)

$$M_y = -\frac{f\tau_x + \frac{\varepsilon^2}{\beta_0}\partial_y\tau_x}{f^2+\varepsilon^2} \tag{3}$$

where f is the Coriolis parameter, ∂_y denotes the meridional derivative, $\beta_0 = 2\Omega/a$ is the gradient of the Coriolis parameter at the equator, ε=5$\times$10^{-6} corresponds to the value of the Coriolis parameter at ϕ=2°, and the zonal surface wind stress is given by

$$\tau_x = \rho_a \mathrm{C_d}|\mathrm{U}|u \tag{4}$$

with air density $\rho_a = 1.2$ kg m^{-3}, drag coefficient $\mathrm{C_d} = 1.3\times10^{-3}$, and surface horizontal zonal wind speed $|\mathrm{U}|$ and wind component u. (Cartesian notation throughout the text is used only for simplicity; calculations are done in spherical coordinates).

The cross-equatorial Ekman mass flux, which has a critical role in the response to asymmetric heating, is independent of ε and given by

$$M_y\big|_{\phi=0} = -\frac{1}{\beta_0}\partial_y\tau_x. \tag{5}$$

c. Forcing

The base atmospheric circulation is driven by Earth's annual-mean insolation profile (solar constant of 1360 Wm^{-2}), without seasonal or diurnal components.

Asymmetric heating is implemented by a prescribed source of ocean heat uptake, given by

$$\nabla\cdot F^S = \begin{cases} -S\cdot\sin\left(4(\phi+5^\circ)\right) & ;40^\circ\mathrm{N}\le\phi\le85^\circ\mathrm{N} \\ -S\cdot\sin\left(4(\phi-5^\circ)\right) & ;85^\circ\mathrm{S}\le\phi\le40^\circ\mathrm{S} \\ 0 & ;\text{otherwise}\end{cases} \tag{6}$$

where F^S denotes the prescribed OET. The prescribed forcing warms the northern hemisphere (NH) and cools the southern hemisphere (SH) but vanishes in the global mean (cf. Kang et al. 2018a,b; Gerstman and Adam 2020); it is analogous to the mean energy transport by AMOC, which accounts for much of the asymmetric heating of the northern hemisphere in the present climate (Marshall et al. 2014), or to the ocean heat loss along western boundary currents in high latitudes (Philander and Fedorov 2003). In the simulations, the prescribed cross-equatorial energy transport F^S scales linearly with S, and is equal to 5.7 PW (1 PW = 10^{15}W) for S=100Wm^{-2} (cf. Kang et al. 2018b).

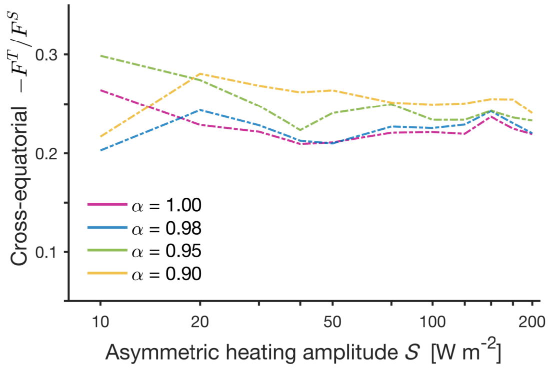

FIG. 3. The dependence of the ratio of the total-cross-equatorial energy transport F^T (given by the sum of the atmospheric and wind-driven oceanic energy transport) and the prescribed cross-equatorial ocean energy transport F^S on the forcing amplitude S and ocean stratification α.

Since F^S is partly balanced by radiative feedbacks, the total energy transport F^T, defined as the sum of AET and the wind-driven OET ($F^T \equiv F^A + F^{Ek}$), is expected to be smaller than F^S. As shown in Fig. 3, the ratio of the cross-equatorial F^T and F^S is roughly 0.25 for a wide range of forcing amplitude and stratification values, indicating that while ~75% of the prescribed heating is balanced by radiative processes, F^T scales linearly with F^S. Therefore, for simplicity, the response to hemispherically-asymmetric heating is presented by its dependence on S.

Previous works have found the ITCZ response to depend on the form of the asymmetric heating. Harrop et al. (2018), Seo et al. (2014), and Green et al. (2019) show increased sensitivity of ITCZ shifts to extratropical heating, compared with the response to tropical heating, due to amplifying effects from cloud and water vapor feedbacks. Yu and Pritchard (2019) found the total energy transport to become more ocean centric as the centers of asymmetric heating are shifted poleward. Similarly, Hilgenbrink and Hartmann (2018) showed that the atmospheric response to prescribed ocean heat uptake is sensitive to how the prescribed energy fluxes affect surface temperature gradients and their associated momentum fluxes. The results shown here may therefore be sensitive to the prescribed forcing profile and to the limitations of the model. Nevertheless, this form of the asymmetric heating is used because it has a minimal effect on surface temperature gradients in the tropical region and hence on the wind-driven dynamic coupling, and for comparability with previous works (in particular Kang et al. 2018a,b; Gerstman and Adam 2020).

d. Observed data

Observed values are taken from the European Center for Medium-Range Weather Forecasts (ECMWF) Interim Reanalysis (ERA-Interim; Dee et al. 2011) for the years 1979–2014. In order to close the atmospheric energy budget, mass-flux corrections are applied to the vertically-integrated fluxes, as described in Trenberth and Fasullo (2012).

e. ITCZ position indices

The latitudes of the precipitation peaks in each hemisphere and of the ITCZ position are calculated using

$$\phi_I = \frac{\int_{\phi_1}^{\phi_2} \phi\,(\cos(\phi)P)^n\,\mathrm{d}\phi}{\int_{\phi_1}^{\phi_2} (\cos(\phi)P)^n\,\mathrm{d}\phi} \tag{7}$$

where P denotes zonal-mean precipitation, ϕ_1 and ϕ_2 denote meridional integration boundaries, and n functions as a smoothing parameter, yielding the precipitation centroid for $n = 1$ and the latitude of maximal precipitation for large n (for a comparison of different ITCZ indices and for a sensitivity analysis of Eq. 7 see Adam et al. 2016a, 2018b). The ITCZ position is defined here as the precipitation centroid, calculated using $n = 1$, $[\phi_1, \phi_2] = [20°\mathrm{S}, 20°\mathrm{N}]$. The northern and southern tropical precipitation peaks are calculated using $n = 10$ and $[\phi_1, \phi_2] = [0, 30°\mathrm{N}]$ and $[30°\mathrm{S}, 0]$, respectively.

f. The energy-flux framework

Assuming that atmospheric transport in the deep tropics is dominated by the mean flow, the ITCZ can be associated with the atmospheric energy flux equator (EFE) – the latitude where column-integrated atmospheric energy transport (AET) diverges and vanishes (Kang et al. 2009; Schneider et al. 2014). Similarly, AET can be assumed to diverge and vanish near IITCZs (Bischoff and Schneider 2016). At steady state, the energy balance equation of the atmosphere becomes

$$\partial_y F^A = \mathrm{NEI}, \tag{8}$$

where atmospheric energy transport F^A is given by the column-integrated meridional flux of moist static energy[5]. Therefore, a Taylor expansion of AET around the equator to third order can be written as

$$F^A \simeq F_0^A + \mathrm{NEI}_0(a\phi) + \tfrac{1}{6}\partial_{yy}\mathrm{NEI}_0(a\phi)^3 \tag{9}$$

where $(\cdot)_0$ denotes equatorial averaging and the second-order term is assumed negligible due to the strong hemispheric asymmetry of AET (Bischoff and Schneider 2016; Adam et al. 2016b). The roots of the third-order expansion (i.e., EFE latitudes) can be categorized into three approximations, based of the value of the discriminant

$$\Delta_I = \mathrm{NEI}_0 + \sqrt[3]{(F_0^A)^2\partial_{yy}\mathrm{NEI}_0} \tag{10}$$

[5]Since column-integrated kinetic energy is relatively small, atmospheric energy transport is dominated by the transport of moist static energy, defined as the sum of moist enthalpy and geopotential energy.

which is dominated by NEI_0 (for a detailed derivation see Bischoff and Schneider 2016; Adam et al. 2016b):

$$\phi_{EFE} \simeq \begin{cases} -\dfrac{1}{a}\dfrac{F_0^A}{\mathrm{NEI}_0} & ; \quad \Delta_I > 0 \quad (11a) \\ -\dfrac{1}{a}\sqrt[3]{\dfrac{6F_0^A}{\partial_{yy}\mathrm{NEI}_0}} & ; \quad \Delta_I \approx 0 \quad (11b) \\ \pm\sqrt{\dfrac{-6\mathrm{NEI}_0}{\partial_{yy}\mathrm{NEI}_0}} & ; \quad \Delta_I < 0 \quad (11c) \end{cases}$$

where for $\Delta_I < 0$, ϕ_{EFE} denotes the approximate latitudes of the two roots on either side of the equator. As shown in Fig. 2a, NEI near the equator is very sensitive to the ocean stratification α, which therefore strongly affects the response of the EFE (and hence the ITCZ) to extratropical heating.

Assuming that ocean energy transport (OET) in the tropics is dominated by the Ekman energy transport F^{Ek}, tropical NEI is given as the balance between net top-of-atmosphere radiative input R^{TOA} and the wind-driven ocean heat uptake $\partial_y F^{Ek}$ (Schneider et al. 2014),

$$\mathrm{NEI} = R^{TOA} - \partial_y F^{Ek}. \quad (12)$$

Taking the leading-order terms in Δ_I and in the fractional changes in the Taylor expansion (9), and empirically accounting for the differences in the displacements of the ITCZ and EFE, the position of the ITCZ can be approximated as

$$\phi_I \simeq \begin{cases} -b_1 F_0^A & ; \quad R_0^{TOA} > \partial_y F_0^{Ek} \ (13a) \\ -b_2\sqrt[3]{F_0^A} & ; \quad R_0^{TOA} \approx \partial_y F_0^{Ek} \ (13b) \\ \pm b_3\sqrt{-\partial_y F_0^A} & ; \quad R_0^{TOA} < \partial_y F_0^{Ek} \ (13c) \end{cases}$$

as summarized in Fig. 4 (Bischoff and Schneider 2016; Adam et al. 2016b). The constants b_1, b_2 and b_3 are empirically determined (e.g., from the seasonal cycle) and may vary across models and climates (Donohoe et al. 2013; Roberts et al. 2017).

Therefore, to leading order, the modality and position of the ITCZ depend on the equatorial values of AET, the radiative budget at the top of the atmosphere and ocean heat uptake. This dependence is predicated on the assumption that atmospheric and oceanic eddy heat transport in the deep tropics can be neglected – an assumption that is not generally justified (Dima et al. 2005; Smith et al. 2006; Roberts et al. 2017; Xiang et al. 2018; Gerstman and Adam 2020). In the idealized GCM, the zonally symmetric boundary conditions eliminate stationary eddy atmospheric and oceanic transport; vertical ocean mixing, which affects ocean heat uptake and stratification, is also absent. Similarly, the radiative budget is missing key elements such as water vapor feedback, cloud radiative effects, and surface albedo feedbacks. The absence of these processes, which undoubtedly have an important role in the real system, nevertheless strengthens the assumptions of energy flux theory in the idealized GCM and allows us to isolate the role of key dynamic mechanisms in the coupled system, which are the focus of the present analysis.

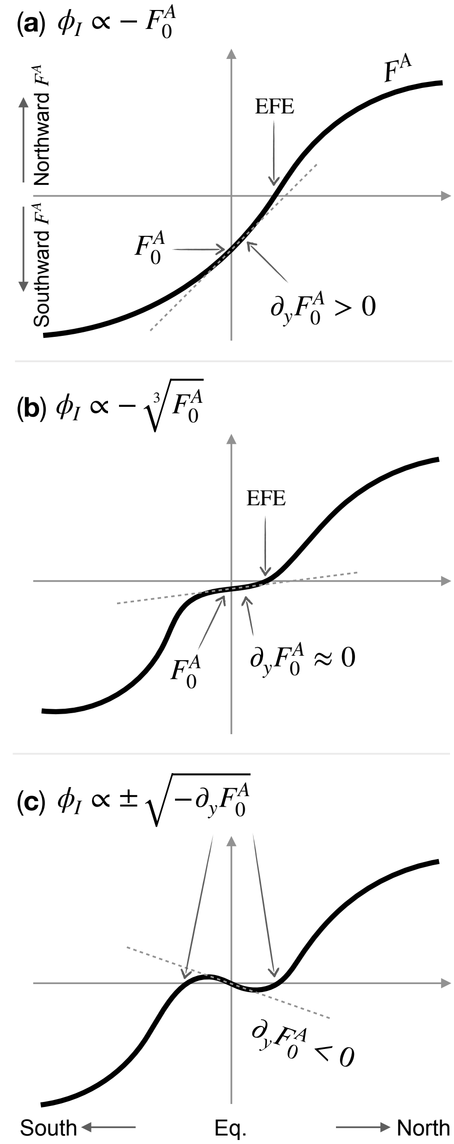

FIG. 4. A depiction of the three approximations of ITCZ positions (ϕ_I, Eq. 13) as roots of the meridional atmospheric energy transport F^A for: (**a**) positive equatorial atmospheric net energy input (NEI) ($\partial_y F_0^A > 0$), (**b**) negligible equatorial NEI ($\partial_y F_0^A \approx 0$), and (**c**) negative equatorial NEI ($\partial_y F_0^A < 0$).

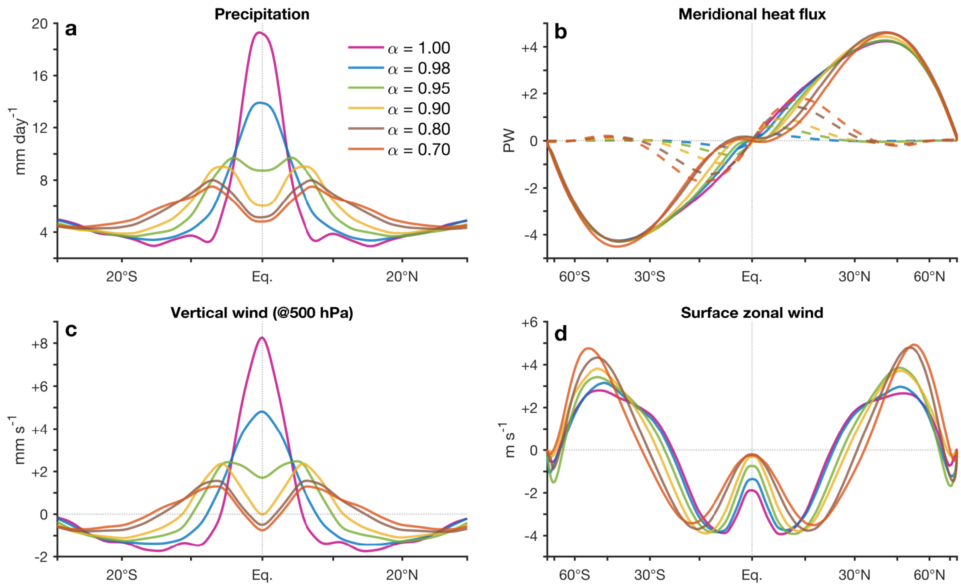

FIG. 5. The dependence on ocean stratification α, for hemispherically symmetric heating, of (**a**) precipitation, (**b**) atmospheric (solid) and oceanic (dashed) meridional energy transport, (**c**) vertical wind at the 500 hPa level, and (**d**) surface zonal wind.

3. Dynamic and energetic constraints on the modality of the ITCZ

In the idealized energy-flux framework, the emergence of IITCZs and their associated anti-Hadley circulation requires that, near the equator, ocean heat uptake be greater than the net radiative input at the top of the atmosphere (i.e., negative NEI_0). From Eq. (10), since cross-equatorial energy fluxes vanish in the hemispherically symmetric case (F_0^A=0), negative NEI_0 is a sufficient condition for the bifurcation to IITCZs in this case (i.e., for $\Delta_I < 0$); for asymmetric heating, lower values of NEI_0 (i.e., increased ocean heat uptake or reduced top-of-atmosphere radiative input) may be required. Therefore, for simplicity, the hemispherically symmetric case is considered first.

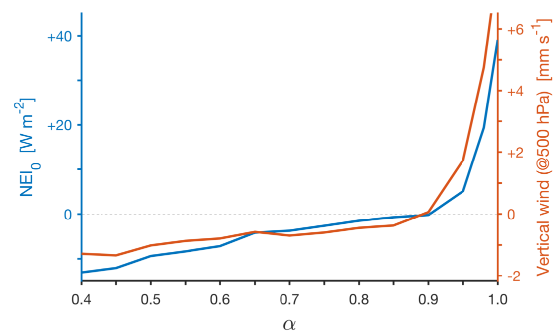

FIG. 6. Dependence on ocean stratification (α) of equatorial atmospheric net energy input (NEI_0, blue) and equatorial vertical wind at the 500 hPa level (orange), for hemispherically symmetric heating. The change from upward to downward (positive to negative) equatorial vertical wind indicates a transition from Hadley to anti-Hadley circulation.

a. Hemispherically symmetric heating

Figure 5 shows the dependence of the idealized GCM on ocean stratification for hemispherically symmetric heating. As ocean stratification increases (i.e., as α decreases), increased equatorial ocean upwelling and cooling (Fig. 2) reduce equatorial precipitation, leading to a doubly-peaked distribution for $\alpha \leq 0.95$, which also widens with decreasing α. Concomitantly, poleward ocean energy transport (OET) increases with ocean stratification (Fig. 5b), leading to a weakening of the Hadley circulation due to the reduced requirement for poleward atmospheric energy transport (AET), as well as reduced tropics-to-extratropics temperature difference (Fig. 2b; Levine and Schneider 2011; Kang et al. 2018b,a; Gerstman and Adam 2020). The weakening of the Hadley circulation, in turn, leads to weakened equatorial easterlies (Fig. 5d). The Hadley circulation also widens with increased ocean stratification, as indicated by the poleward shift of the subtropical latitudes where the zonal-mean surface wind changes from easterlies to westerlies, thereby extending the region of easterly stress (Levine and Schneider 2011; Kang et al. 2018b). Thus, the effect of the coupled atmospheric and wind-driven ocean circulations on the distribution of tropical precipitation involves both local and global dynamic processes (Levine and Schneider 2011; Tomas et al. 2016; Green and Marshall 2017;

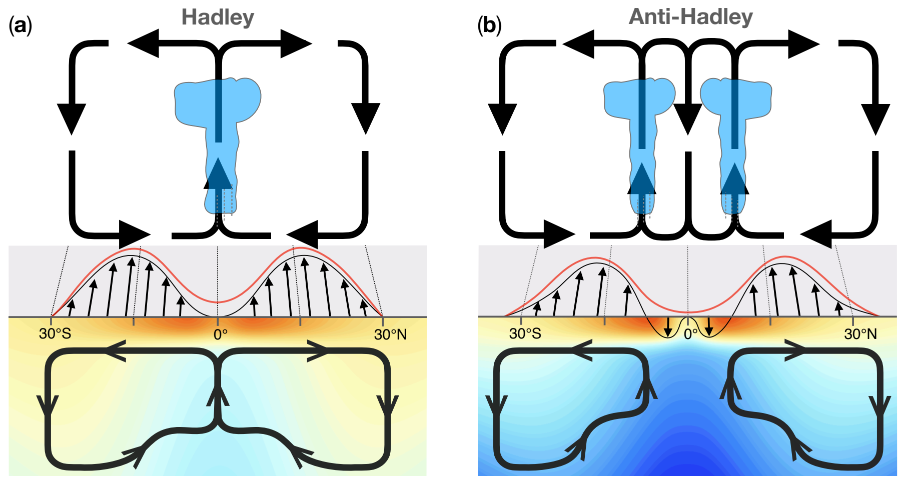

FIG. 7. Depiction of the coupled atmospheric (upper panels) and wind-driven ocean circulations (lower panels) for (**a**) Hadley and (**b**) anti-Hadley circulation, neglecting zonally asymmetric processes. Thin red lines indicate the easterly surface stress. The thin black lines and arrows indicate the geostrophically-balanced component of the surface stress. The difference between the thin red and black lines near the equator can be interpreted as momentum diffusion (D_x in Eq. 14). The vertical color gradients in the lower panels depict differences in ocean stratification, which is stronger in panel **b**. The increased ocean stratification leads to the equatorial cooling required to sustain the anti-Hadley circulation. The surface winds associated with the anti-Hadley circulation, in turn, broaden the upwelling region and shallow the thermocline (which follows the lower boundary of the subtropical cells) below the double ITCZs. The weakened surface stress of the anti-Hadley circulation weakens the Ekman mass transport, thereby moderating the increase in Ekman energy transport with increased ocean stratification (Eq. 1).

Kang et al. 2018a; Green et al. 2019; Kang 2020). Locally, wind-induced evaporation and ocean energy transport affect the tropical SST distribution, and with it the precipitation distribution. The changes in tropics-to-extratropics temperature gradients caused by the wind-driven circulation, affect the tropical mean overturning circulation intensity and extent, which, in turn, modulates the tropical winds.

The sensitivity of the tropical precipitation to ocean stratification differs for relatively weak ($\alpha > 0.9$) and strong ($\alpha < 0.9$) stratification, showing reduced sensitivity as α decreases (Gerstman and Adam 2020). The largest change in the sensitivity occurs when the Hadley circulation bifurcates to an anti-Hadley circulation for $\alpha < 0.9$, as indicated by the negative equatorial vertical winds for $\alpha < 0.9$ (Fig. 6). This change in the sensitivity can be explained by considering the statistically-steady zonal-mean surface zonal momentum balance,

$$v\partial_y u - fv = D_x - \tau_x \tag{14}$$

where v and u denote the meridional and zonal components of the surface wind, τ_x is the wind stress by the zonal-mean wind (Eq. 4), and D_x represents diffusion of surface momentum not related to mean surface stress (e.g., convective damping, eddy stress and vertical advection of momentum). As depicted in Fig. 7a, the surface equatorward winds of the Hadley circulation develop easterly stress which drives equatorial upwelling and increased equatorial ocean heat uptake. In contrast, the poleward surface winds of the anti-Hadley circulation develop a geostrophic westerly component (Fig. 7b) which reduces both the amplitude and meridional gradient of the easterly stress near the equator (Fig. 5d). This moderates the increase in wind-driven Ekman transport (Fig. 5b) and ocean heat uptake (Eq. 1) with increasing ocean stratification (Gerstman and Adam 2020).

In the case of hemispherically symmetric heating, since v, $\partial_y u$ and f vanish near the equator, $\tau_x \approx D_x$ there. Therefore, if the momentum diffusion D_x is weak, anti-Hadley circulation cannot intensify because it represses the easterly stress required to sustain the equatorial upwelling (and hence the ocean heat uptake) which leads to negative equatorial atmospheric NEI (Eqs. 10 and 11). This negative feedback explains the nonlinear dependence of equatorial NEI on α, seen in Figs. 2a and 6. In the absence of ocean stratification ($\alpha = 1$), NEI is maximal at the equator. As α decreases, equatorial NEI dramatically reduces until it turns negative. The bifurcation to anti-Hadley circulation, which occurs when equatorial NEI turns negative, represses the easterly stress in the deep tropics, preventing from ocean heat uptake to increase with ocean stratification and therefore from equatorial NEI to be further reduced. Thus, the negative feedback limits the extent and intensity of anti-Hadley circulation and its associated IITCZs.

The weakening of the Hadley circulation in the idealized model with increasing ocean stratification is shown in Fig. 8. For reference, the hemispherically symmetric component of the observed annual-mean atmospheric meridional overturning circulation is shown in Fig. 8a. For a

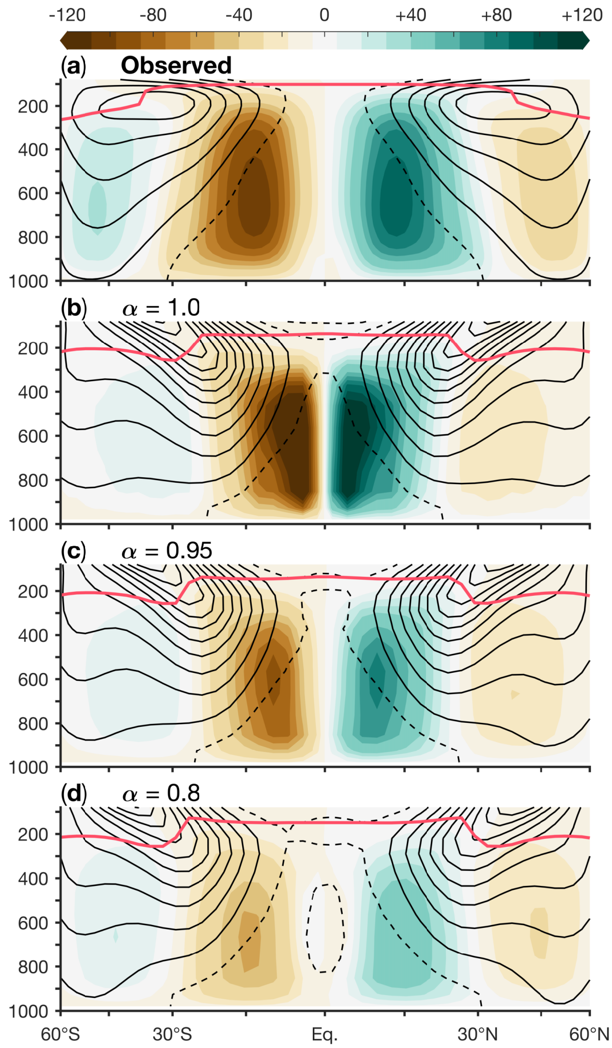

FIG. 8. The mass streamfunction (color contours, in units of Sv = 10^9kg s^{-1}) and zonal-mean zonal wind (black contours at intervals of 5m s^{-1}; dashed line indicate negative values), for: (**a**) the hemispherically-symmetric component of the annual-mean observed circulation; the idealized GCM forced with annual-mean insolation and (**b**) $\alpha = 1$ (static slab ocean), (**c**) $\alpha = 0.95$ and (**d**) $\alpha = 0.8$. The tropopause is indicated by a red line. Observed values are taken from the ERA-Interim reanalysis for the years 1979–2014.

static slab ocean (α=1) the Hadley circulation is significantly stronger than observations (Fig. 8b; cf. Levine and Schneider 2011). Values comparable to the observed circulation are obtained for $\alpha = 0.95$. For $\alpha = 0.8$, a weak anti-Hadley circulation is seen in the deep tropics, with weakened Hadley-like cells poleward of the anti-Hadley circulation.

b. Hemispherically asymmetric heating

The response of the atmospheric circulation in the idealized GCM to increased ocean stratification with hemispherically asymmetric heating (S=100Wm^{-2}) is shown in Fig. 9, decomposed to equatorially-symmetric (middle panels) and cross-equatorial (right panels) components. The observed atmospheric meridional overturning circulation during July-August is shown for reference in the top panels (Fig. 9a–c). A more dramatic weakening of the cross-equatorial circulation is seen with increased stratification, compared with the symmetric component. In addition, a stronger anti-Hadley circulation emerges for weaker stratification than in the symmetric heating case (Fig. **??** vs. Fig. 5c).

Figure 10 shows the dependence of the idealized GCM on ocean stratification for hemispherically asymmetric heating (S=100Wm^{-2}). For α=1 a single precipitation peak is seen at about 6°N (Fig. 10a). As α decreases, a bimodal precipitation distribution appears at weaker stratification ($\alpha \leq$0.95) than for hemispherically-symmetric heating ($\alpha \leq$0.9). Similarly, negative equatorial NEI and the bifurcation to anti-Hadley circulation occurs at higher α (0.95 in Fig. 10c,d vs. 0.9 in Figs. 5c, 2a). With increasing stratification, the meridional gradient of the zonal surface wind at the equator, and hence of the zonal wind stress τ_x, weakens. This weakens the cross-equatorial Ekman mass transport M_y (Eq. 5), thereby moderating the increase in cross-equatorial OET with decreasing α (Gerstman and Adam 2020).

The reduced stratification threshold for bifurcation to anti-Hadley circulation can be explained by the existence of cross-equatorial mass and energy transport. For hemispherically asymmetric heating, the advection term $v\partial_y u$ (which vanishes in the symmetric case) is generally positive (i.e., v and $\partial_y u$ have the same sign; Fig. 10e,f), requiring increased easterly stress (Eq. 14 for fixed D_x). This weakens the negative feedback caused by the geostrophic westerly tendency of the surface winds of the anti-Hadley circulation. Similarly, cross-equatorial AET increases the value of the discriminant Δ_I (the second term on the rhs of Eq. 10 is a definite positive for an equatorial minimum in NEI). Therefore, lower values of equatorial NEI are required for bifurcation to anti-Hadley circulation to occur (i.e., for $\Delta_I < 0$). This leads to twice as large negative values of equatorial NEI, compared to the symmetric case ($\sim$-20Wm^{-2} in Fig.10d vs. $\sim$-10Wm^{-2} in Fig. 1a), contributing to the intensified anti-Hadley circulation and IITCZs in the asymmetric heating case.

Thus, in the idealized GCM, the modality of the precipitation distribution is set by the intensity of the equatorial cooling, which is coupled to the atmospheric overturning circulation in a complex manner. In the following section the quantification of ITCZ shifts is considered, taking into account the modality of the precipitation distribution.

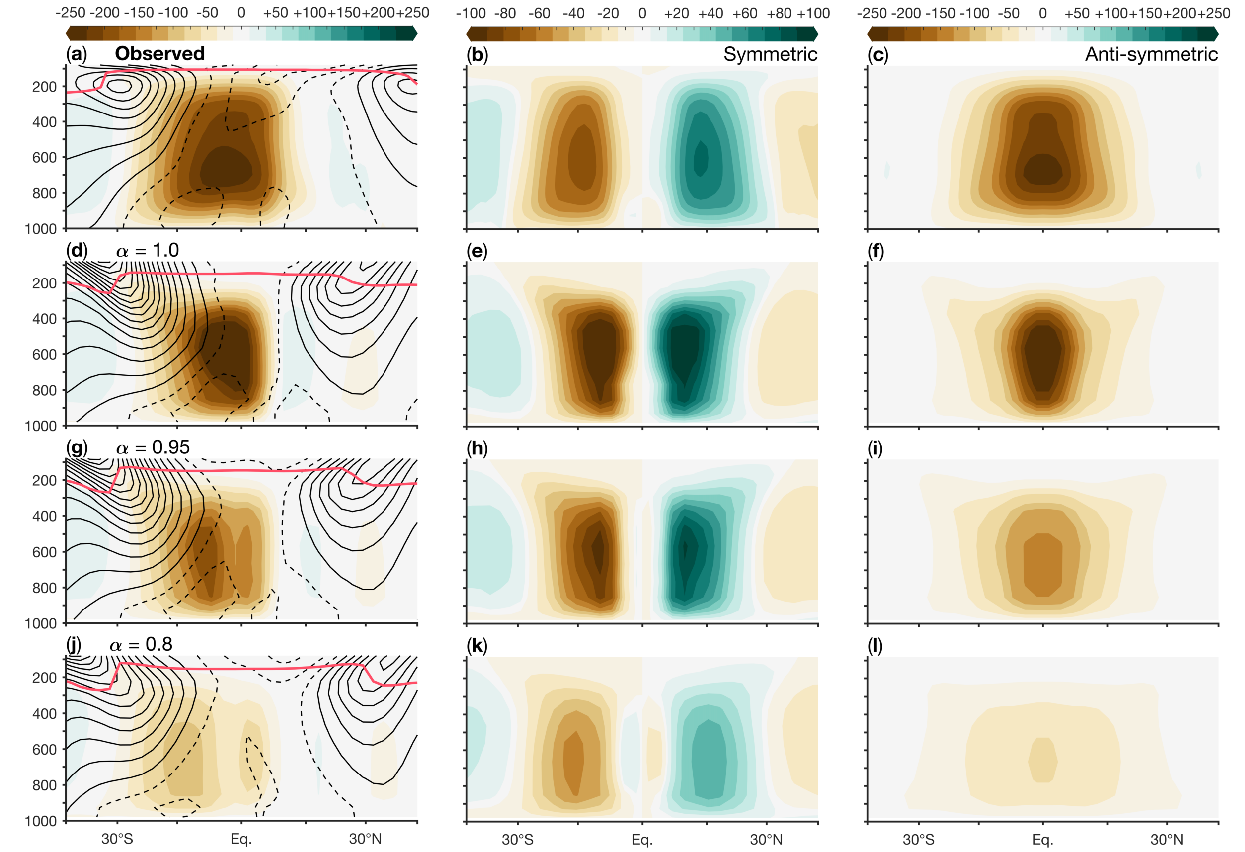

FIG. 9. The mass streamfunction (in units of Sv = 10^9kg s^{-1}, left panels), decomposed to equatorially-symmetric (ψ^{ES} middle panels) and cross-equatorial (ψ^{CE} right panels) components for (**a**,**b**,**c**) the observed circulation during July-August; the idealized model forced with S =100Wm^{-2} and (**d**,**e**,**f**) $\alpha = 1$ (static slab ocean), (**g**,**h**,**i**) $\alpha = 0.95$ and (**j**,**k**,**l**) $\alpha = 0.8$. Observed values are taken from the ERA-Interim reanalysis for 1979–2014. The equatorially-symmetric and and cross-equatorial components of the streamfunctions are calculated as $\psi^{ES} = \frac{1}{2}\left[\psi(\phi) - \psi(-\phi)\right]$ and $\psi^{CE} = \frac{1}{2}\left[\psi(\phi) + \psi(-\phi)\right]$.

4. Dynamic and energetic constraints on the position of the ITCZ

a. Using $P - E$ to determine transitions from ITCZ to IITCZ states

Figure 11a shows the dependence of the zonal-mean precipitation on α for hemispherically symmetric heating. For α=1, a single peak is seen on the equator. As α decreases, the precipitation distribution becomes increasingly bimodal. For hemispherically symmetric heating, the precipitation centroid, a commonly-used metric for the ITCZ position, is at the equator for all α. It therefore captures the ITCZ position when the distribution is unimodal (i.e., for weak stratification) but does not reveal important information about the positions of the off-equatorial precipitation peaks when the distribution is bimodal. Distinguishing between unimodal and bimodal precipitation distributions is therefore critical for quantifying shifts of the ITCZ.

The bifurcation to anti-Hadley circulation, seen as a change from mean equatorial ascent to descent, marks the transition to a strongly bimodal distribution of the tropical precipitation (i.e., to IITCZs; Fig. 11b). Specifically, the change in sign of the equatorial vertical wind is related only to the equatorially-symmetric component of the circulation (the anti-symmetric component is identically zero at the equator). While the vertical wind and equatorial NEI are quantities closely linked to the transition to IITCZs (Fig. 11b,c), these are not readily obtained in observations. In the idealized GCM, the transition to IITCZ (i.e., to descending equatorial winds, Fig. 11b) occurs when precipitation minus evaporation ($P - E$) has an equatorial minimum lower than 1 mm day^{-1} (Fig. 11d). We therefore use $P_0 - E_0 \leq$1mm day^{-1} as a criterion for transitions from ITCZ to IITCZ states – a criterion that is readily carried over to other datasets, and is more robust than selecting a cutoff value of equatorial precipitation, which may vary across climates.

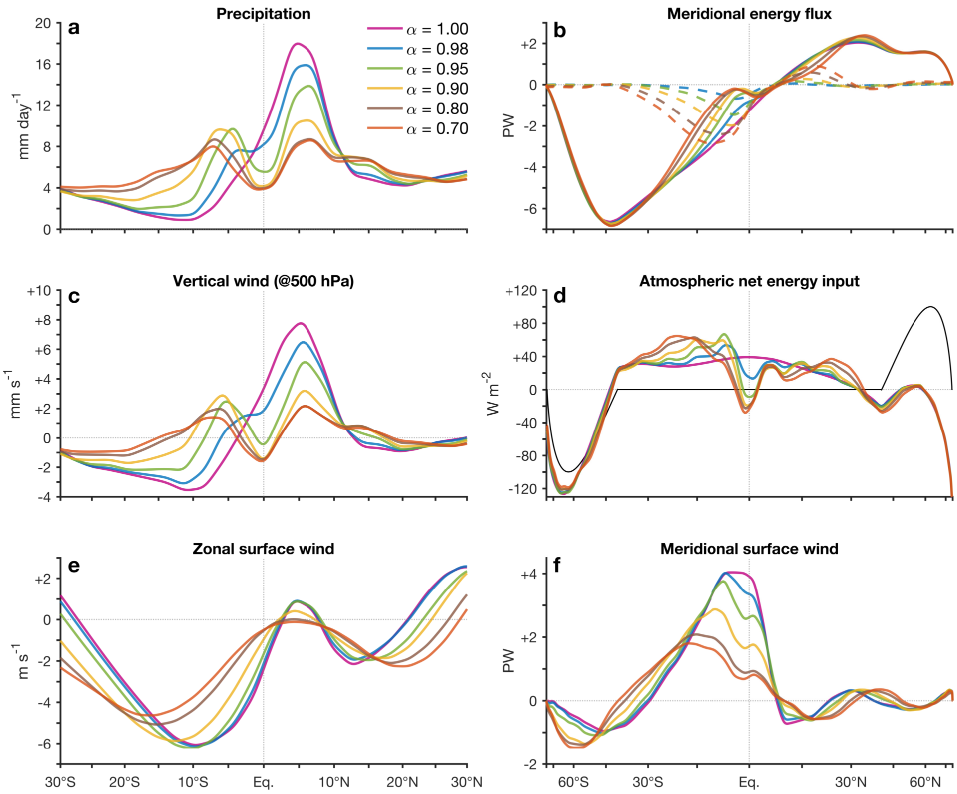

FIG. 10. The dependence on ocean stratification α, for hemispherically asymmetric heating (S =100Wm^{-2}), of the zonal-mean (**a**) precipitation, (**b**) atmospheric (solid) and oceanic (dashed) meridional energy transport, (**c**) vertical wind at the 500 hPa level, (**d**) atmospheric net energy input, (**e**) surface zonal wind, and (**f**) surface meridional wind. The prescribed atmospheric heating is shown in panel **d** (black line).

The dependence of the zonal-mean $P-E$ field on asymmetric heating is shown in Fig. 12. For weak stratification ($\alpha > 0.95$), $P-E$ is unimodal in the tropics. Consistent with the previous section, a bifurcation to IITCZ occurs as α decreases (due to increased equatorial cooling); the critical value of α at which the bifurcation occurs increases with the amplitude of asymmetric heating (due to cross-equatorial momentum and energy transport). For $\alpha \leq 0.9$, consistent with Eq. 13c, the IITCZs are approximately equally displaced off the equator; however, the precipitation is stronger in the warmer hemisphere (northern ITCZ). Next we examine the response of ITCZ positions to changes in ocean stratification and asymmetric heating, while taking into account changes in the modality of the ITCZ.

b. Calculating the ITCZ position

The dependence of the precipitation centroid and of the precipitation peaks that straddle the equator on the asymmetric heating is shown in Fig. 13a,b. As shown in previous studies, shifts of the precipitation centroid are damped with increasing ocean stratification (Green and Marshall 2017; Kang et al. 2018a,b; Green et al. 2019; Gerstman and Adam 2020). In contrast, the poleward shift of the precipitation peaks is amplified for weak ocean stratification (α >0.95), and becomes insensitive to the asymmetric heating for strong stratification ($\alpha \leq$0.95). For α=0.9, the northern and southern peaks are both at about 6° latitude for all values of the forcing amplitude S. Therefore, for strong stratification, the poleward shift of the precipitation centroid reflects changes in the relative strength of the northern vs. southern peaks rather than ITCZ shifts.

Interestingly, the latitude of the energy flux equator (ϕ_{EFE}) is found to be well captured by the cubic root of the forcing amplitude S, and independent of ocean stratification (Fig. 13c). This points to the cubic root approximation (Eq. 13b, Fig. 4b) as a potentially useful approximation over a wide range of climates. However, the redundancy with respect to ocean stratification might also point to a weakness of the energy-flux framework, or of the idealized GCM. In particular, using a similar idealized GCM, Gerstman and Adam (2020) found that cross-equatorial AET by transient eddies accounts for the differences between the EFE and the precipitation centroid, which can be significant. Since the categories of empirical approximations of the ITCZ positions (Eq. 13, Fig. 4) are determined primarily by $\partial_y F_0^A$ (i.e., equatorial NEI,

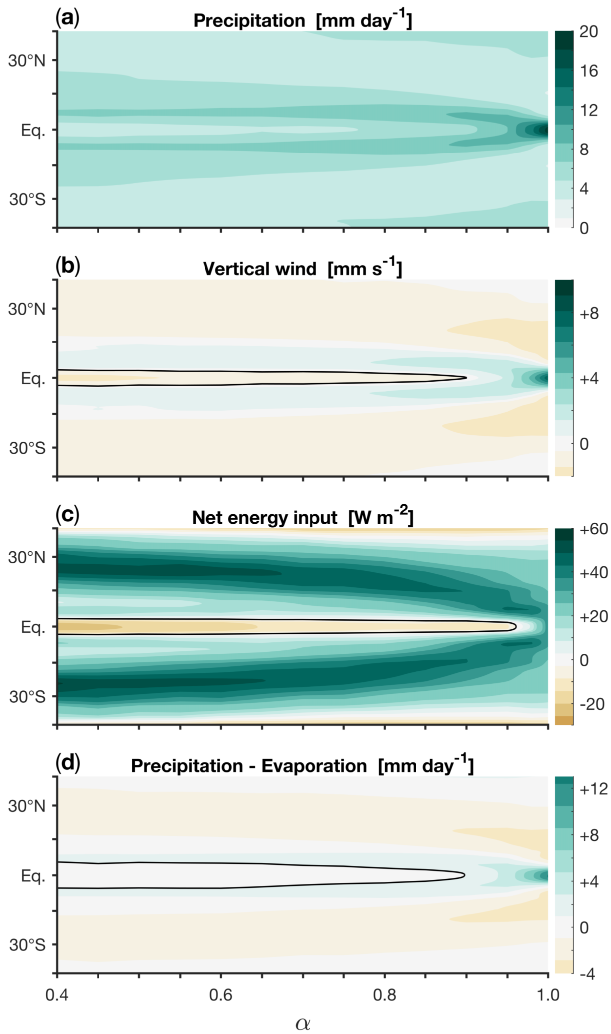

FIG. 11. Dependence on ocean stratification α, for hemispherically symmetric heating, of the zonal-mean (**a**) precipitation, (**b**) vertical wind (at 500 hPa), (**c**) atmospheric net energy input (NEI), and (**d**) precipitation minus evaporation. Black lines indicate the zero vertical wind and NEI contours and the precipitation minus evaporation = 1 mm day^{-1} contour closest to the equator.

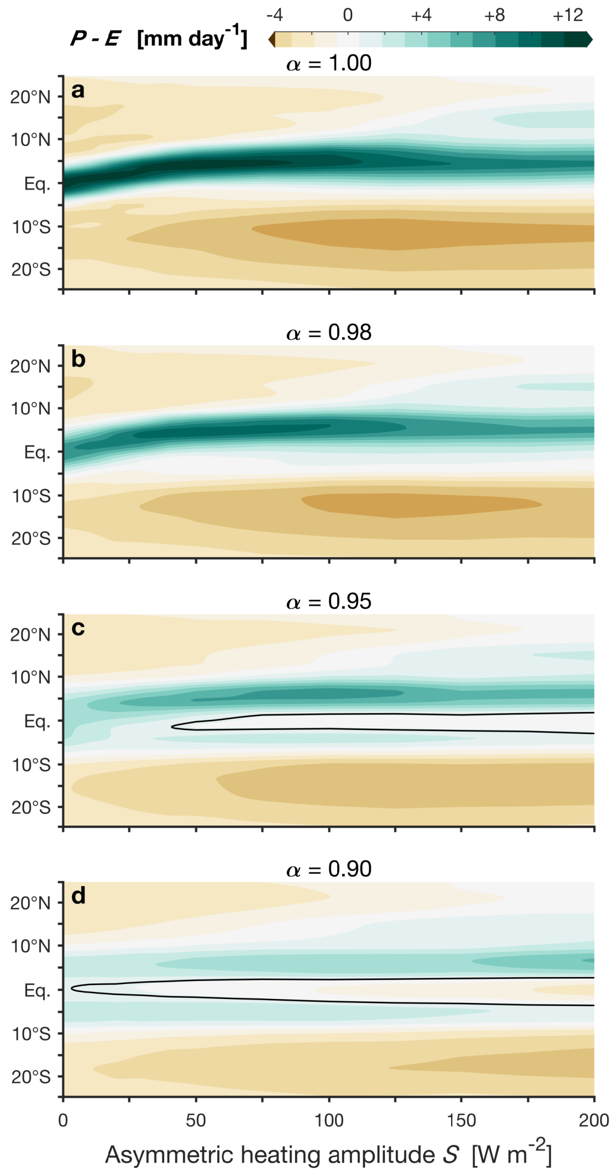

FIG. 12. Dependence on asymmetric heating amplitude S of precipitation minus evaporation for (**a**) α=1, (**b**) α=0.98, (**c**) α=0.95, and (**d**) α=0.9. Black lines indicate the precipitation minus evaporation = 1 mm day^{-1} contour closest to the equator.

Eq. 11), we next examine the sensitivity of $\partial_y F_0^A$ in the tropics to the asymmetric heating and ocean stratification.

As shown in Fig. 14a, for a static ocean (α=1), the gradient of AET in the tropics is approximately constant and positive, justifying a linear approximation of the EFE and ITCZ positions (Fig. 4a). For weak stratification ($\alpha = 0.98$, Fig. 14b), the AET gradient remains positive, but an inflection point is seen near the equator. Therefore, for weak stratification, the linear approximation may be justified only over a limited range of cross-equatorial AET (F_0^A) values. Given that a similar near-equator inflection point is seen in the observed AET in the tropics (Fig. 14b, black lines), this points to the limitations of the commonly-used linear approximation in analyses of the observed and simulated climate. For stronger stratification ($\alpha = 0.95$, Fig. 14c), the AET gradient approximately vanishes near the equator for $S <$100Wm^{-2}, justifying a cubic root approximation (Fig. 4b), and becomes negative for $S \geq$100 Wm^{-2}, justifying a IITCZ approximation (Fig.4c).

Fig. 15 shows the relation of the precipitation centroid (colors) to the first-order EFE approximation (Eq. 11a, dashed) and to empirical best-fits of the linear (Eq. 13a, dotted) and cubic-root (Eq. 13b, solid) approximations.

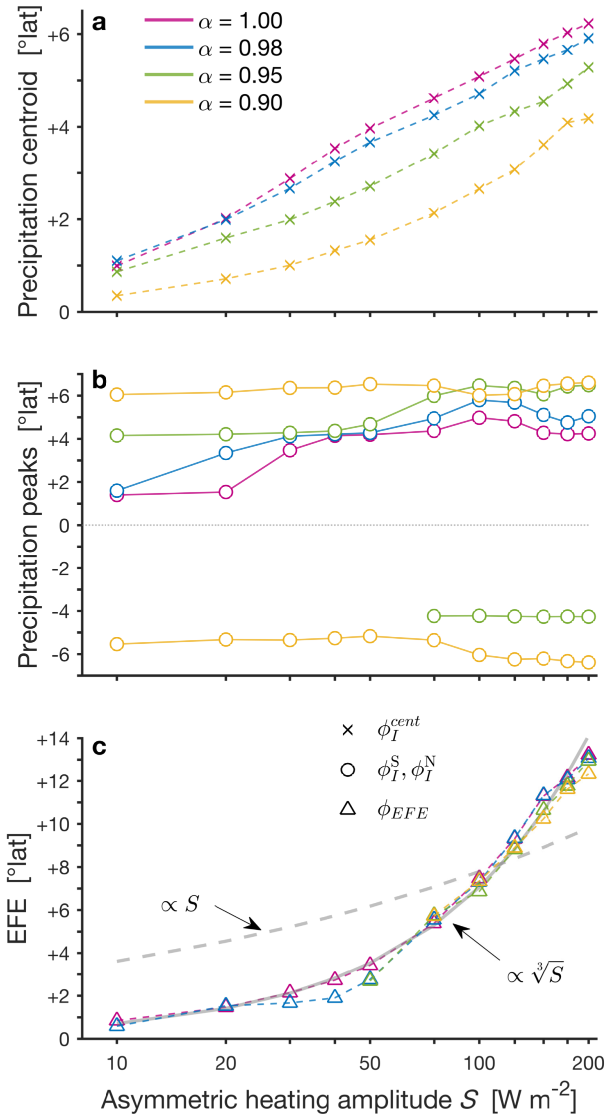

FIG. 13. Dependence on asymmetric heating amplitude S and on ocean stratification α of (**a**) the precipitation centroid, (**b**) precipitation peaks north (ϕ_I^N) and south (ϕ_I^S) of the equator, and (**c**) the energy flux equator (ϕ_{EFE}). The latitudes of the precipitation centroid and of the precipitation peaks are calculated using Eq. (7). Linear and cubic root best fits of ϕ_{EFE} vs. S are shown in gray dashed and solid lines.

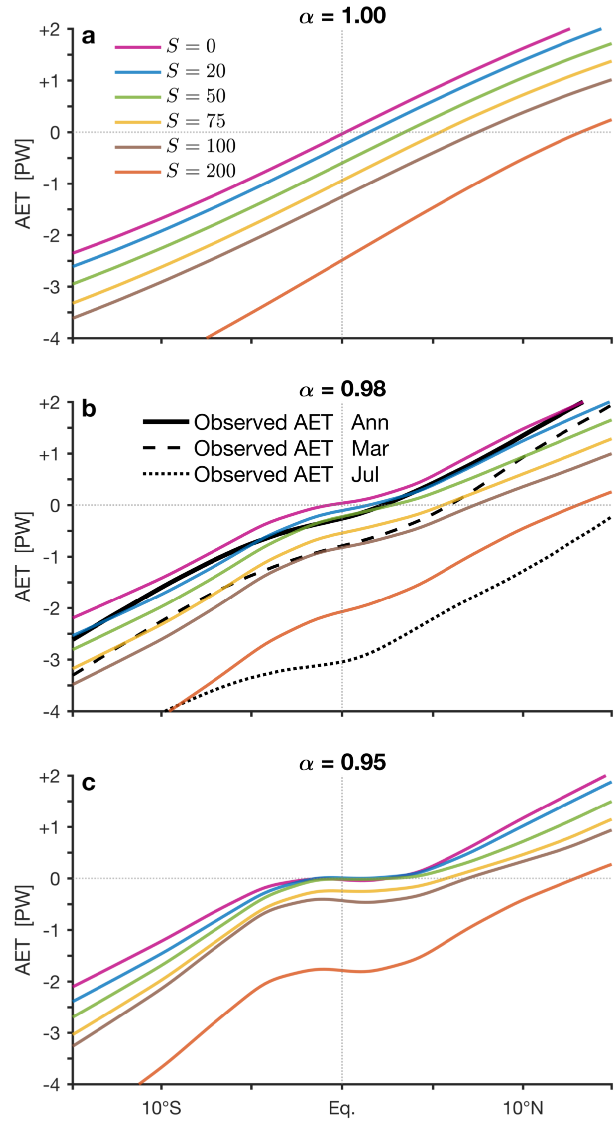

FIG. 14. Dependence of tropical zonal-mean atmospheric energy transport (AET) on the amplitude of the asymmetric heating S (Wm^{-2}) for ocean stratification (α) values: (**a**) 1.00, (**b**) 0.98 and (**c**) 0.95. Observed AET profiles for the annual-mean (solid black), March (dashed black) and July (dotted black) are shown for reference in panel **b**. Observed values are taken from the ERA-Interim reanalysis for 1979–2014.

As for the case of the EFE (Fig. 13c), the cubic-root approximation clearly best captures the variations in the precipitation centroid. In addition, for different α values, the fractional variations in the empirical constant of the cubic approximation are significantly smaller than for the linear approximation (b_2 varies by less than 7% for α =0.95–1.00; b_1 varies by nearly 20% for α =0.98–1.00). The comparison between the different approximations suggests that, over a wide range of climates, (i) empirical models based on the cubic approximation may capture the position of the ITCZ better than the commonly-used linear approximation, and (ii) variations in equatorial NEI ($\partial_y F_0^A$) play a secondary role to cross-equatorial AET.

5. Discussion and summary

An idealized GCM with parameterized Ekman ocean energy transport (OET) is used to study the effect of wind-driven OET on the modality of the zonal-mean tropical precipitation distribution, and on shifts of the ITCZ.

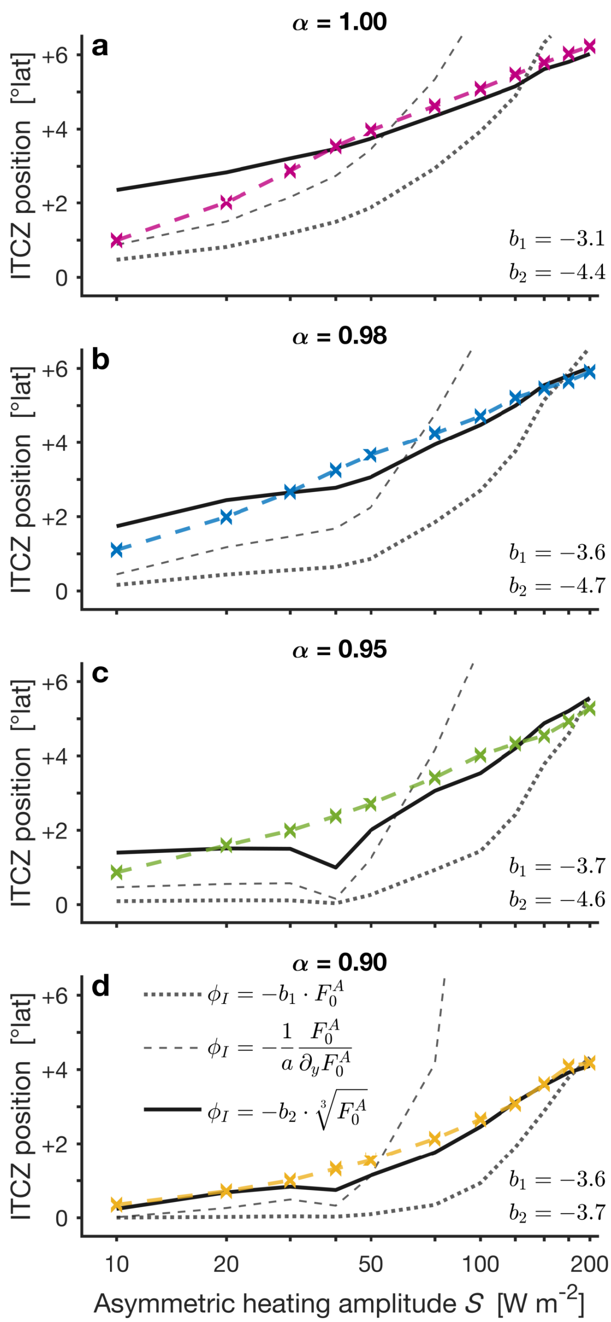

FIG. 15. Dependence of the precipitation centroid (dashed crosses) and of the various approximations of the ITCZ position on the amplitude of the asymmetric heating S for ocean stratification (α) values: (**a**) 1.00, (**b**) 0.98,(**c**) 0.95, and (**d**) 0.90. Dotted lines show the empirical linear approximation (Eq. 13a, Fig. 4a). Solid lines show the empirical cubic approximation (Eq. 13b, Fig. 4b). Dashed lines show the first-order energy flux equator approximation (Eq. 11a). The values of the coefficients b_1 and b_2 are shown for each α.

In the idealized GCM, transitions from unimodal to bimodal distributions are driven by increased equatorial ocean upwelling and cooling, which inhibits equatorial precipitation. These transitions go along with a bifurcation from Hadley (single ITCZ) to anti-Hadley circulation, with an equatorial descending branch and rising branches (IITCZs) that straddle the equator (Bischoff and Schneider 2016). An equatorial minimum in precipitation minus evaporation ($P-E$) below 1 mm day^{-1} is found to be a simple and robust criterion for transitions to unimodal to bimodal distributions (i.e., from Hadley to anti-Hadley circulation), across a range of ocean stratification and asymmetric heating values.

The intensity and extent of the anti-Hadley circulation, and hence of the IITCZs, is constrained by a negative feedback. The poleward surface winds of the anti-Hadley circulation develop a westerly geostrophic component (Figs. 1 and 7) that weakens the easterly stress which drives equatorial cooling. Therefore, in the absence of external sources of easterly stress (which may come from eddy diffusion or momentum advection), anti-Hadley cells and their associated IITCZs cannot intensify. Indeed, for asymmetric heating, meridional advection of zonal momentum near the equator allows the anti-Hadley circulation to emerge for lower values of ocean stratification and to further intensify, reaching intensities about twice as large as in the hemispherically-symmetric case for forcing amplitude $S = 100$ Wm^{-2}.

Since the easterly stress in the observed climate is primarily due to the seasonal cycle of the Hadley circulation (Lee 1999), the negative IITCZ feedback suggests increased prevalence and intensity of IITCZs in high obliquity climates. This prediction is consistent with reported results of aquaplanet simulations with a dynamic ocean, showing reduced equatorial atmospheric net energy input (NEI) with increased obliquity (Ferreira et al. 2014). In the idealized GCM, the transition from unimodal to bimodal precipitation distribution is forced by increasing the prescribed ocean stratification, which increases ocean heat uptake in the equatorial upwelling region (Fig. 7; Kang et al. 2018a,b; Gerstman and Adam 2020). In more realistic systems, these changes can be driven by various processes that reduce equatorial NEI, such as cloud radiative feedbacks and enhanced ocean turbulent vertical mixing. Nevertheless, to the extent that Ekman transport dominates ocean energy transport and uptake in the deep tropics, the sensitivity found in the idealized GCM can be expected to hold in more realistic systems.

The precipitation modality critically affects the response of the ITCZ to asymmetric heating. Specifically,

1. For weak ocean stratification, which goes along with one dominant precipitation peak, the wind-driven OET damps shifts of the tropical precipitation centroid but amplifies shifts of the precipitation peak (Fig. 13).

2. For strong ocean stratification, which goes along with pronounced IITCZs, shifts of the precipitation centroid are strongly damped; in contrast, the IITCZs are found farther from the equator. In this case, the response of the IITCZs to asymmetric heating is characterized by relative intensification of the precipitation peak in the warming hemisphere, rather than meridional shifts.

The damped response of the precipitation centroid with increasing stratification is attributed to the partitioning of cross-equatorial energy transport between the atmosphere and ocean (Schneider et al. 2014; Green and Marshall 2017; Schneider 2017; Kang et al. 2018a,b; Green et al. 2019; Gerstman and Adam 2020; Kang 2020). In contrast, the amplified shifts of the precipitation peaks are due to the extended equatorial cooling which shifts the regions of maximal sea surface temperatures poleward (Lindzen and Nigam 1987; Philander et al. 1996; Clement 2006). These competing paradigms highlight the importance of metric selection in analyses of tropical precipitation variations. In particular, the generally accepted idea of damped (or 'sticky') ITCZ response in coupled models applies *only* to the precipitation centroid. Since shifts of precipitation peaks can be amplified by coupled dynamics, the concept of a damped response may be inappropriate or even misleading for impact studies.

Similarly, the idealized paradigm of a tropical Hadley circulation with a single ITCZ is commonly used to guide analyses of tropical precipitation. However, as shown here, consideration of the tropical precipitation modality is important for understanding changes in the position, intensity and width of the ITCZ (Byrne et al. 2018). For example, in the zonal mean, the notorious double ITCZ bias in modern climate models is characterized primarily by relative intensification of the precipitation peak in the southern hemisphere, with only slight shifts of the precipitation peaks in either hemisphere, compared with observations (Lin 2007; Adam et al. 2016c, 2018a). This matches the sensitivity to asymmetric heating found here for a strongly bimodal precipitation distribution. Analyses that takes into account biases in the modality of the tropical precipitation may therefore be better posed to provide insight on the nature and origin of the problem.

Due to the equatorial cooling by ocean upwelling, and due to the negative feedback of the anti-Hadley circulation that prevents it from intensifying, atmospheric NEI is constrained to relatively small values near the equator (Fig. 6). In the limit of vanishing equatorial NEI, which at steady state is equal to the gradient of atmospheric energy transport (AET) at the equator, the energy-flux framework predicts that the position of the ITCZ is proportional to the cubic root of the cross-equatorial AET (Fig. 4b, Eq. 11). As shown in Fig. 15, the cubic root approximation is indeed found to capture the sensitivity of the precipitation centroid to asymmetric heating over a wide range of asymmetric heating amplitudes and ocean stratification values significantly better than the commonly-used linear approximation (for all values of α, $R<0.5$ for the linear approximation vs. $R>0.8$ for the cubic-root approximation). This suggests that the cubic-root approximation may be more appropriate when shifts of the ITCZ are considered over a wide range of climates.

The results presented here span a wide range of asymmetric heating and stratification values, but a relatively limited range of mean global temperatures (20 $\pm$2.4C$^\circ$ across all simulations). Levine and Schneider (2011) found that as the climate warms, the importance of OET diminishes due to the weakening of the equator to pole temperature difference and of the Hadley circulation. Aside for the apparent limitations of the idealized model, the sensitivity to ocean stratification found here, which seems to be relevant to the present climate (Figs. 9, 10,14), might therefore differ for significantly warmer or colder climates. Moreover, cloud radiative effects, which are not present in the idealized model, may significantly alter the sensitivity of IITCZs to asymmetric heating and ocean stratification (Popp and Silvers 2017), even in cases of strong ocean stratification.

While the subtropical cells vary on decadal timescales, wind-driven ocean energy transport involves processes that span seasonal to millennial time scales (Yu and Pritchard 2019; Kang 2020). Understanding the coupled response of the tropical rain belt to asymmetric heating therefore requires further analysis using a hierarchy of reduced-complexity coupled models, on various time scales.

Acknowledgments. This work was supported by the Israeli Science Foundation grant 1185/17. I thank Maya Samuals and Moran Erez for their helpful comments. The code for the idealized GCM is publicly available at *https://github.com/tapios/fms-idealized*.

References

Adam, O., 2018: Zonally varying ITCZs in a Matsuno–Gill-type model with an idealized Bjerknes feedback. *Journal of Advances in Modeling Earth Systems*, **10 (6)**, 1304–1318, doi:10.1029/2017MS001183.

Adam, O., T. Bischoff, and T. Schneider, 2016a: Seasonal and interannual variations of the energy flux equator and ITCZ. Part I: Zonally averaged ITCZ position. *J. Climate*, **29**, 3219–3230, doi: 10.1175/JCLI-D-15-0512.1.

Adam, O., T. Bischoff, and T. Schneider, 2016b: Seasonal and interannual variations of the energy flux equator and ITCZ. Part II: Zonally varying shifts of the ITCZ. *J. Climate*, **29**, 7281–7293, doi: 10.1175/JCLI-D-15-0710.1.

Adam, O., T. Schneider, and F. Brient, 2018a: Regional and seasonal variations of the double-ITCZ bias in CMIP5 models. *Climate Dynamics*, **51**, 101–117, doi:10.1007/s00382-017-3909-1.

Adam, O., T. Schneider, F. Brient, and T. Bischoff, 2016c: Relation of the double-ITCZ bias to the atmospheric energy budget in climate models. *Geophys. Res. Lett.*, **43**, 7670–7677.

Adam, O., and Coauthors, 2018b: The TropD software package (v1): standardized methods for calculating tropical-width diagnostics. *Geosci. Model Dev.*, **11**, 4339–4357, doi:10.5194/gmd-11-4339-2018.

Back, L. E., and C. S. Bretherton, 2009: On the relationship between SST gradients, boundary layer winds, and convergence over the tropical oceans. *Journal of Climate*, **22 (15)**, 4182–4196, doi:10.1175/2009JCLI2392.1.

Barreiro, M., A. Fedorov, R. Pacanowski, and S. G. Philander, 2008: Abrupt climate changes: how freshening of the northern atlantic affects the thermohaline and wind-driven oceanic circulations. *Annu. Rev. Earth Planet. Sci.*, **36**, 33–58.

Bischoff, T., and T. Schneider, 2014: Energetic constraints on the position of the Intertropical Convergence Zone. *J. Climate*, **27**, 4937–4951, doi:10.1175/JCLI-D-13-00650.1.

Bischoff, T., and T. Schneider, 2016: The equatorial energy balance, ITCZ position, and double ITCZ bifurcations. *J. Climate*, **29**, 2997–3013, doi:10.1175/JCLI-D-15-0328.1.

Bjerknes, J., 1969: Atmospheric teleconnections from the equatorial Pacific. *Mon. Wea. Rev.*, **97**, 163–172.

Blackburn, M., and Coauthors, 2013: The aqua-planet experiment (ape): Control sst simulation. *Journal of the Meteorological Society of Japan. Ser. II*, **91A**, 17–56, doi:10.2151/jmsj.2013-A02.

Byrne, M. P., A. G. Pendergrass, A. D. Rapp, and K. R. Wodzicki, 2018: Response of the intertropical convergence zone to climate change: Location, width, and strength. *Current Climate Change Reports*, **4 (4)**, 355–370, doi:10.1007/s40641-018-0110-5.

Clement, A. C., 2006: The role of the ocean in the seasonal cycle of the Hadley circulation. *J. Atmos. Sci.*, **63**, 3351–3365.

Codron, F., 2012: Ekman heat transport for slab oceans. *Clim. Dyn.*, **38**, 379–389.

Colose, C. M., A. N. LeGrande, and M. Vuille, 2016: Hemispherically asymmetric volcanic forcing of tropical hydroclimate during the last millennium. *Earth System Dynamics*, **7 (3)**, 681–696.

Czaja, A., and J. Marshall, 2006: The partitioning of poleward heat transport between the atmosphere and ocean. *Journal of the atmospheric sciences*, **63 (5)**, 1498–1511.

Dee, D., and Coauthors, 2011: The ERA-Interim reanalysis: configuration and performance of the data assimilation system. *Quart. J. Roy. Meteor. Soc*, **137**, 553–597.

Dima, I. M., J. W. Wallace, and I. Kraucunas, 2005: Tropical zonal momentum balance in the NCEP reanalyses. *J. Atmos. Sci.*, **62**, 2499–2513.

Donohoe, A., J. Marshall, D. Ferreira, and D. McGee, 2013: The relationship between ITCZ location and cross-equatorial atmospheric heat transport: From the seasonal cycle to the last glacial maximum. *J. Climate*, **26**, 3597–3618.

Emanuel, K., 2005: Increasing destructiveness of tropical cyclones over the past 30 years. *Nature*, **436**, 686–688.

Ferreira, D., J. Marshall, P. A. O'Gorman, and S. Seager, 2014: Climate at high obliquity. *Icarus*, **in press**.

Frierson, D. M. W., I. M. Held, and P. Zurita-Gotor, 2006: A gray-radiation aquaplanet moist GCM. Part I: Static stability and eddy scale. *J. Atmos. Sci.*, **63**, 2548–2566.

Gerstman, H., and O. Adam, 2020: Nonlinear damping of itcz migrations due to ekman ocean energy transport. *Geophysical Research Letters*, **accepted**.

Green, B., and J. Marshall, 2017: Coupling of trade winds with ocean circulation damps itcz shifts. *J. Climate*, **30**, 4395–4411, doi:10.1175/JCLI-D-16-0818.1.

Green, B., J. Marshall, and J.-M. Campin, 2019: The 'sticky' itcz: ocean-moderated itcz shifts. *Climate Dynamics*, **53 (1)**, 1–19, doi:10.1007/s00382-019-04623-5, URL https://doi.org/10.1007/s00382-019-04623-5.

Harrop, B. E., J. Lu, F. Liu, O. A. Garuba, and L. Ruby Leung, 2018: Sensitivity of the ITCZ location to ocean forcing via q-flux green's function experiments. *Geophysical Research Letters*, **45 (13)**, 116 – 13, doi:10.1029/2018GL080772.

Hartmann, D. L., 1994: *Global Physical Climatology*, International Geophysics Series, Vol. 56. Academic Press, San Diego, CA, USA, 418 pp.

Held, I. M., 2001: The partitioning of the poleward energy transport between the tropical ocean and atmosphere. *J. Atmos. Sci.*, **58**, 943–948.

Hilgenbrink, C. C., and D. L. Hartmann, 2018: The response of hadley circulation extent to an idealized representation of poleward ocean heat transport in an aquaplanet gcm. *Journal of Climate*, **31 (23)**, 9753–9770, doi:10.1175/JCLI-D-18-0324.1.

Kang, S. M., 2020: Extratropical influence on the tropical rainfall distribution. *Current Climate Change Reports*, 1–13.

Kang, S. M., D. M. W. Frierson, and I. M. Held, 2009: The tropical response to extratropical thermal forcing in an idealized GCM: The importance of radiative feedbacks and convective parameterization. *J. Atmos. Sci.*, **66**, 2812–2827.

Kang, S. M., Y. Shin, and F. Codron, 2018a: The partitioning of poleward energy transport response between the atmosphere and ekman flux to prescribed surface forcing in a simplified gcm. *Geoscience Letters*, **5 (1)**, 22, doi:10.1186/s40562-018-0124-9.

Kang, S. M., Y. Shin, and X. X.P., 2018b: Extratropical forcing and tropical rainfall distribution: energetics framework and ocean ekman advection. *npj Climate and Atmospheric Science*, **1 (1)**, doi:10.1038/s41612-017-0004-6.

Lee, S., 1999: Why are the climatological zonal winds easterly in the equatorial upper troposphere? *J. Atmos. Sci.*, **56**, 1353–1363.

Levine, X. J., and T. Schneider, 2011: Response of the Hadley circulation to climate change in an aquaplanet GCM coupled to a simple representation of ocean heat transport. *J. Atmos. Sci.*, **68**, 769–783.

Lin, J.-L., 2007: The double-ITCZ problem in IPCC AR4 coupled GCMs: Ocean–atmosphere feedback analysis. *J. Climate*, **20**, 4497–4525.

Lindzen, R. S., and S. Nigam, 1987: On the role of sea surface temperature gradients in forcing low-level winds and convergence in the Tropics. *J. Atmos. Sci.*, **44**, 2418–2436.

Lutsko, N. J., J. Marshall, and B. Green, 2019: Modulation of monsoon circulations by cross-equatorial ocean heat transport. *Journal of Climate*, **32 (12)**, 3471–3485.

Marshall, J., A. Donohoe, D. Ferreira, and D. McGee, 2014: The ocean's role in setting the mean position of the Inter-Tropical Convergence Zone. *Clim. Dyn.*, **42**, 1967–1979, doi:10.1007/s00382-013-1767-z.

McCreary, J. P., and P. Lu, 1994: Interaction between the subtropical and equatorial ocean circulations: The subtropical cell. *J. Phys. Oceanogr.*, **24**, 466–497.

Mechoso, C. R., and Coauthors, 1995: The seasonal cycle over the tropical pacific in coupled ocean-atmosphere general circulation models. *Mon. Wea. Rev.*, **123**, 2825–2838.

Medeiros, B., B. Stevens, and S. Bony, 2015: Using aquaplanets to understand the robust responses of comprehensive climate models to forcing. *Climate Dynamics*, **44 (7–8)**, 1957–1977, doi:10.1007/s00382-014-2138-0.

Möbis, B., and B. Stevens, 2012: Factors controlling the position of the intertropical convergence zone on an aquaplanet. *J. Adv. Model. Earth Syst.*, **4**, M00A04, doi:10.1029/2012MS000199.

O'Gorman, P. A., and T. Schneider, 2008: The hydrological cycle over a wide range of climates simulated with an idealized GCM. *J. Climate*, **21**, 3815–3832.

PAGES Hydro2k Consortium, 2017: Comparing proxy and model estimates of hydroclimate variability and change over the common era. *Climate of the Past*, **13 (12)**, 1851–1900, doi:10.5194/cp-13-1851-2017, URL https://cp.copernicus.org/articles/13/1851/2017/.

Philander, S., and A. Fedorov, 2003: Role of tropics in changing the response to Milankovich forcing some three million years ago. *Paleoceanography*, **18 (2)**, 1045, doi:10.1029/2002PA000837.

Philander, S., D. Gu, D. Halpern, G. Lambert, N. Lau, T. Li, and R. Pacanowski, 1996: Why the ITCZ is mostly north of the equator. *J. Climate*, **9**, 2958–2972.

Popp, M., and S. Bony, 2019: Stronger zonal convective clustering associated with a wider tropical rain belt. *Nature communications*, **10 (1)**, 1–12.

Popp, M., and L. G. Silvers, 2017: Double and single ITCZs with and without clouds. *Journal of Climate*, **30 (22)**, 9147–9166.

Privé, N. C., and R. A. Plumb, 2007: Monsoon dynamics with interactive forcing. Part I: Axisymmetric studies. *J. Atmos. Sci.*, **64**, 1417–1430.

Roberts, W., P. Valdes, and J. Singarayer, 2017: Can energy fluxes be used to interpret glacial/interglacial precipitation changes in the tropics? *Geophysical Research Letters*, **44 (12)**, 6373–6382.

Schneider, T., 2004: The tropopause and the thermal stratification in the extratropics of a dry atmosphere. *J. Atmos. Sci.*, **61**, 1317–1340.

Schneider, T., 2017: Feedback of atmosphere-ocean coupling on shifts of the intertropical convergence zone. *Geophysical Research Letters*, **44 (22)**, 11–644.

Schneider, T., T. Bischoff, and G. H. Haug, 2014: Migrations and dynamics of the intertropical convergence zone. *Nature*, **513**, 45–53, doi:10.1038/nature13636.

Seo, J., S. M. Kang, and D. M. W. Frierson, 2014: Sensitivity of intertropical convergence zone movement to the latitudinal position of thermal forcing. *J. Climate*, **27 (8)**, 3035–3042, doi:10.1175/JCLI?D?13?00691.1.

Smith, R. S., C. Dubois, and J. Marotzke, 2006: Global climate and ocean circulation on an aquaplanet ocean–atmosphere general circulation model. *Journal of climate*, **19 (18)**, 4719–4737.

Sumi, A., 1992: Pattern formation of convective activity over the aquaplanet with globally uniform sea surface temperature (sst). *Journal of the Meteorological Society of Japan. Ser. II*, **70 (5)**, 855–876, doi:10.2151/jmsj1965.70.5_855.

Swenson, M., and D. Hansen, 1999: Tropical pacific ocean mixed layer heat budget: The pacific cold tongue. *J. Phys. Oceanogr.*, **29**, 69–81.

Talib, J., S. Woolnough, N. Klingaman, and C. Holloway, 2018: The role of the cloud radiative effect in the sensitivity of the intertropical convergence zone to convective mixing. *J. Climate*, **31**, 6821–6838, doi:10.1175/JCLI-D-17-0794.1.

Tomas, R. A., C. Deser, and L. Sun, 2016: The role of ocean heat transport in the global climate response to projected arctic sea ice loss. *Journal of Climate*, **29**, 6841–6859, doi:10.1175/JCLI-D-15-0651.1.

Trenberth, K. E., and J. T. Fasullo, 2012: Tracking Earth's energy: From El Niño to global warming. *Surv. Geophys.*, **33**, 413–426.

Voigt, A., S. Bony, J.-L. Dufresne, and B. Stevens, 2014a: The radiative impact of clouds on the shift of the intertropical convergence zone. *Geophys. Res. Lett.*

Voigt, A., B. Stevens, J. Bader, and T. Mauritsen, 2014b: Compensation of hemispheric albedo asymmetries by shifts of the ITCZ and tropical clouds. *J. Climate*, **27**, 1029–1045.

Xiang, B., M. Zhao, Y. Ming, W. Yu, and S. M. Kang, 2018: Contrasting impacts of radiative forcing in the southern ocean versus southern tropics on itcz position and energy transport in one gfdl climate model. *Journal of Climate*, **31 (14)**, 5609–5628.

Yu, S., and M. S. Pritchard, 2019: A strong role for the amoc in partitioning global energy transport and shifting itcz position in response to latitudinally discrete solar forcing in cesm1. 2. *Journal of Climate*, **32 (8)**, 2207–2226.

Zhang, C., 2001: Double ITCZs. *J. Geophys. Res.*, **106**, 785–11 792.

Zheng, Y., J.-L. Lin, and T. Shinoda, 2012: The equatorial Pacific cold tongue simulated by IPCC AR4 coupled GCMs: Upper ocean heat budget and feedback analysis. *J. Geophys. Res.*, **117**, C05 024, doi:10.1029/2011JC007746.